ChemComm

Accepted Manuscript

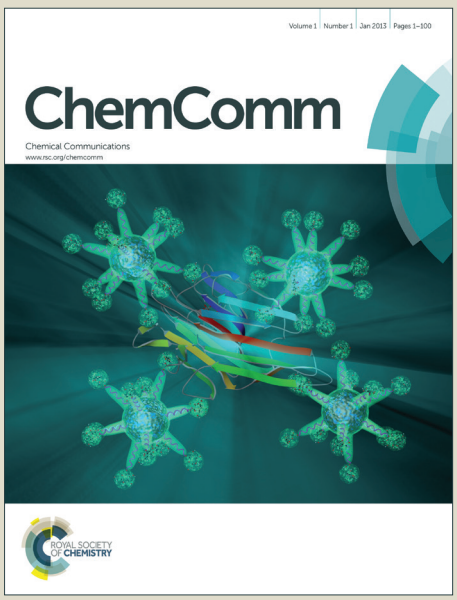

ROYAL SOCIETY OF CHEMISTRY

www.rsc.org/chemcomm

Cite this: DOI: 10.1039/c0xx00000x

www.rsc.org/xxxxxx

ARTICLE TYPE

Surfactant-free Synthesis of GeO_2 Nanocrystals with Controlled Morphologies

Morteza Javadi, Zhenyu Yang and Jonathan G. C. Veinot*

Received (in XXX, XXX) Xth XXXXXXXXX 20XX, Accepted Xth XXXXXXXXX 20XX

DOI: 10.1039/b000000x

Germanium dioxide has many applications in the optoelectronics sector and is the subject of substantial research interest. In this contribution we report the preparation of germanium dioxide nanoparticles of varied sizes and morphologies using a facile sol-gel methodology that requires no addition of templating agents (e.g., surfactants). Morphological control is achieved by tailoring the reaction mixture water/ethanol ratio, ammonium hydroxide concentration, time, and temperature.

Germanium dioxide is a high-k dielectric[1,2] and its phase stability below 425 °C [3] makes it an ideal system for the electronics industry.[4,5] In addition, photoluminescence (PL) from GeO_2 nanostructures (e.g., nanowires) has been demonstrated with peak energies at ca. 3.1 eV (400 nm) and 2.2 eV (563.6 nm).[6-8] The origin of this PL has been attributed to oxygen vacancies, or other surface defects.[7,9-12] However, this intriguing property remains the subject of extensive study. Much of the curiosity directed toward GeO_2 nanostructures arises from how it differs from its Si counterpart (i.e., SiO_2); for example, in addition to its higher dielectric constant (i.e., ε_{GeO2} = 14.5 vs. ε_{SiO2} = 3.9),[1,2,5] it also has a higher refractive index (η_{GeO2} = 1.6-1.65 vs. η_{SiO2} = 1.45),[13,14] wider optical transparency window between 280 and 5000 nm (i.e., from UV to near IR area),[15] and a higher linear coefficient of thermal expansion.[16] All of these properties make germanium dioxide nanostructures appealing for a wide range of applications including, optical waveguides,[17] connections in optoelectronic communications,[6,9,18-20] photosensors,[21] among others.[22-24]

GeO_2 nanostructures have been synthesized *via* sol-gel reactions using tetraethoxygermane (TEOG)[25] or tetrachlorogermane.[15,26,27] Unlike the analogous reactions of tetraethoxysilane used to prepare Stöber silica, direct sol-gel reactions using TEOG or $GeCl_4$ are rapid and difficult to control/study.[13] As a result, when GeO_2 nanostructures of tailored size and/or morphology are targeted it is necessary to include substantial quantities of capping agents (i.e., surfactants) to achieve the desired product.[13,26,28-32]

While the addition of surfactants facilitates some shape control, these additives are often costly, can influence reaction pathways, and complicate material purification. Furthermore, if the GeO_2 nanostructures are intended as precursors for other nanomaterials (e.g., Ge NPs)[25] even traces of these seemingly inert impurities could lead to contamination. In this regard, a surfactant-free synthetic approach to well-defined GeO_2 nanostructures of tailored morphologies is clearly appealing. Herein, we report a straightforward method for forming GeO_2 NPs of controlled size and shape. Our approach does not require addition of any templating agents or surfactants, and achieves morphological tailoring yielding small pseudospherical nanoparticles, eggs, spindles, and nanocubes of GeO_2.

The synthetic methods employed for all of the presented materials are described in detail in the electronic supplemental information and generally involve controlled hydrolysis and condensation of TEOG. Briefly, addition of TEOG to a water/ethanol solution of ammonium hydroxide with rapid stirring yields a cloudy white suspension. Following aging the resulting white product was isolated *via* centrifugation, washed repeatedly with anhydrous ethanol, and dried *in vacuo* at 110 °C for 12 hours. Defining the water/ethanol ratio, ammonium hydroxide concentration, as well as reaction time and temperature yields different particle morphologies and assemblies. The following discussion focuses on the influences of these parameters on the evolution of the GeO_2 particles.

The Influence of Water/Ethanol Ratio: The dependence of GeO_2 NP morphology on the reaction media water/ethanol ratio for reactions catalyzed by 10^{-3} M ammonium hydroxide is illustrated well in the scanning and transmission electron microscopy evaluation of the isolated products (See Figs. 1 and S1). Small (13 nm ± 21%) pseudospherical GeO_2 NPs are obtained when the volume percentage of water (vol. %) is 10 (Figs. 1A, B and S1A, B). These small particles are agglomerated, consistent with the present reaction conditions that do not involve the addition of surface capping agents. Increasing the water content to 30 vol. % yields egg-shaped (length = 525 nm ± 9%; width = 325 nm ± 13%, Figs. 1C, D and S1C, D) assemblies of the small particles noted in Fig. 1A. GeO_2 spindles (length = 250 nm ± 23%; width = 175 nm ± 18%, Figs. 1E, F and S1E, F) with rough surfaces are obtained when reactions are performed at 50 vol. % water. These spindles are similar to those prepared using reverse micelle templates by Jiang *et al.*[28] and Kawai *et al.*[29] Interestingly, contrast in the transmission electron microscopy images is consistent with the present spindles being hollow (Figure 1F, S1E). The exact mechanism for the formation of these hollow structures remains unclear and is the subject of

ongoing study in our laboratory. Finally, upon addition of sufficient water (i.e., > 70 vol. %), well-defined GeO_2 nanocubes with edge dimensions of 314 nm ± 10% are obtained (Figure 1G, H).

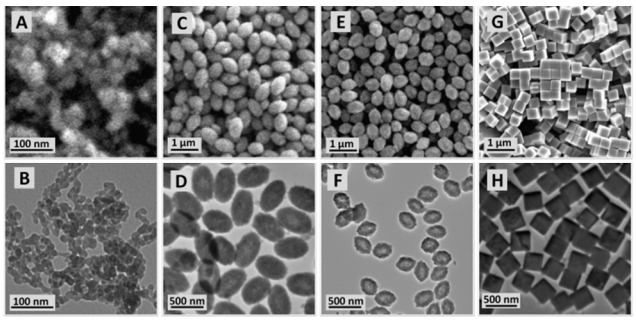

Figure 1. SEM and brightfield TEM images of GeO_2 NPs prepared using indicated water/ethanol ratios: **A, B)** Small pseudospherical NPs (10 vol. % H_2O); **C, D)** Eggs (30 vol. % H_2O); **E, F)** Spindles (50 vol. % H_2O); **G, H)** Nanocubes (>70 vol. % H_2O).

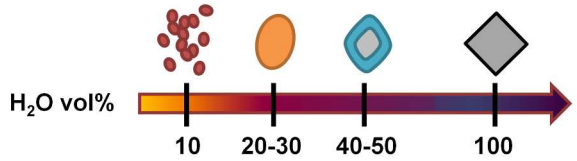

Scheme 1. A schematic summary of the morphological evolution of GeO_2 NPs resulting from changes in the water/ethanol ratio for the sol-gel reaction of TEOG when catalyzed by 10^{-3} M ammonium hydroxide.

Scheme 1 summarizes the influence of the vol. % H_2O in the reaction mixture on GeO_2 NP shape when the reaction is catalyzed by 10^{-3} M ammonium hydroxide. The observed evolution of particle morphology may be understood in the context of TEOG hydrolysis and condensation, combined with a general nucleation and growth mechanism.[33] According to Eq. 1, hydrolysis of TEOG begins with the formation of $Ge(OC_2H_5)_{4-x}(OH)_x$. The exact product distribution obtained from this reaction will depend upon the water/ethanol ratio (i.e., vol. % H_2O). With increasing vol. % H_2O, "x" will tend toward 4 resulting in $Ge(OH)_4$ being the dominant product. The hydrolysis product mixture (i.e., $Ge(OC_2H_5)_{4-x}(OH)_x$, x = 1, 2, 3, 4) subsequently participates in condensation reactions (Eq. 2) and yields materials whose properties (i.e., morphology) are expected to depend upon the original hydrolysis product distribution.

$$Ge(OC_2H_5)_4 + xH_2O \rightleftharpoons Ge(OC_2H_5)_{4-x}(OH)_x + xC_2H_5OH \quad Eq.1$$

$$Ge(OC_2H_5)_{4-x}(OH)_x \rightleftharpoons Ge(OC_2H_5)_{4-x}(O)_{x/2} + (x/2)H_2O \quad Eq.\ 2$$

At low vol. % water, it is reasonable that x<<4. Under these conditions there are few reactive sites where condensation can occur and particle formation/growth will proceed slowly. This is consistent with our experimental observation that ca. 2 hours is required for a cloudy suspension to form when the reaction mixture vol. % water = 10. In this context, it is reasonable to expect the particle size to be limited by reaction time and available water; small particles will result. When the vol. % water approaches 30, small GeO_2 colloids form more rapidly because more sites are available for condensation reactions to occur. Under these conditions it is reasonable that particles will come together forming loosely agglomerated assemblies that subsequently crosslink through further surface-surface condensation reactions. This process will yield covalently linked aggregate particle assemblies like those shown in Figs. 1C and D. A similar process is expected to occur at higher vol. % water (i.e., 50%) to yield bonded structures (see Figure 1E, F). At vol. % water greater than 70 well-defined crystalline cubes are formed. The formation and characterization of these nanocubes will be the subject of the following discussion.

Representative energy dispersive X-ray (EDX) analysis shown in Figure 2 confirms the presence of germanium and oxygen in all NPs presented here. Interestingly, no N is detected at the sensitivity of EDX indicating negligible ammonium hydroxide contamination. IR spectra of all GeO_2 morphologies are nearly identical (See Fig. S2) with a strong absorption at ca. 895 cm^{-1} that is readily attributed to vibration modes of GeO_4 tetrahedra.[21] X-ray powder diffraction (XRD, Figure 2) confirms all nanoparticles, regardless of size or morphology exhibit the hexagonal GeO_2 (α-GeO_2) crystal structure [PDF #04-0498].[34,38] Peak broadening in the XRD patterns of small nanoparticles, eggs and spindles (which are assemblies of small particles) is consistent with small crystalline domains. Nanocubes show sharp intense signals consistent with their comparatively large size determined using electron microscopy. Electron diffraction of a single nanocube (Figure 2 C) shows a pattern consistent with a single crystal domain. It has previously been reported that the most thermodynamically stable crystal planes of α-GeO_2 are (1-11), (011) and (10-1). In this context, cube-like nanocrystals terminated by these faces are reasonable.[28] Representative high-resolution transmission electron microscopy (HRTEM) analysis of a single nanocube (Figure S3) shows lattice fringes separated by 0.34 nm consistent with the α-GeO_2 (10-1) and (011) planes.[38]

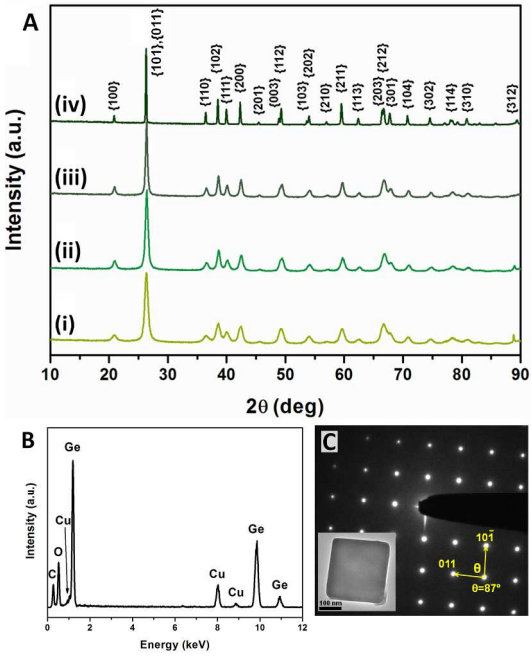

Figure 2. **A)** XRD patterns of different GeO_2 NPs morphologies. **i.** pseudospherical particles, **ii.** eggs, **iii.** spindles, and **iv.** Nanocubes; **B)** A representative EDX spectra for all GeO_2 NPs morphologies; **C)** A representative Selected Area Electron Diffraction (SAED) pattern of a single GeO_2 nanocube (inset).

The Influence of Ammonium Hydroxide and TEOG Concentration.

Having established the optimum vol. % water for the formation of GeO_2 crystalline nanocubes (i.e., 100%), we turn our attention to the ammonium hydroxide concentration while maintaining the water content and TEOG concentration constant. Figure 3 shows the influence of NH_4OH concentration on GeO_2 nanocube morphology. For 0.003 M NH_4OH, polydisperse GeO_2 nanocubes (edge = 350 nm ± 18%, Fig. 3A) are obtained. For 0.01 M NH_4OH the product is dominated by well-defined GeO_2 nanocubes (i.e., 314 nm ± 10%: Figs. 3B, C, E). Increasing the NH_4OH to 0.03 M provides polyhedral particles and nanocubes that appear fused presumably because of surface-surface condensation reactions noted above (Fig. 3D).

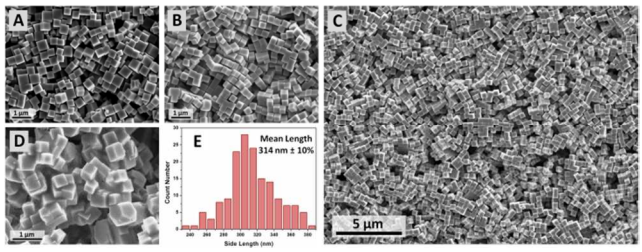

Figure 3. Morphological changes of GeO_2 nanocubes as a function of ammonium hydroxide concentration. **A)** 0.003 M, 350 nm ± 18%; **B,C,E)** 0.011 M, 314 nm ± 10%, and **D:** 0.03 M, 287 nm ± 33%.

Recall, that under the presented conditions TEOG is expected to be completely converted to $Ge(OH)_4$ (*vide supra*). In this context, ammonium hydroxide impacts the acid/base equilibria of $Ge(OH)_4$ as outlined in Eq. 3 and 4.[36]

$$Ge(OH)_4 + H_2O \rightleftharpoons Ge(OH)_3O^- + H_3O^+ \quad pK_{a1} = 9.3 \quad Eq.3$$

$$Ge(OH)_3O^- + H_2O \rightleftharpoons Ge(OH)_2O^{2-} + H_3O^+ \quad pK_{a2} = 12.4 \quad Eq.4$$

The present observations indicate ammonium hydroxide concentration influences particle shape, however elucidating the exact sol-gel mechanism of particle formation/evolution is difficult given the constantly evolving distribution of germania sources (e.g., $Ge(OH)_4$, $Ge(OH)_3O^-$, $Ge(OH)_2O_2^{2-}$, etc.) that results from numerous combinations of hydrolysis and condensation reactions. Complicating interpretation, these reactions will also induce changes in the pH of the reaction media, which are known to impact sol-gel processes.[35]

Considering the equilibrium presented in Eq. 3 and the initial pH of the reaction media (i.e., pH >10), it is expected that all of the $Ge(OH)_4$ will be deprotonated to form $Ge(OH)_3O^-$. According to Eq. 4 negligible $Ge(OH)_3O^-$ will be converted to $Ge(OH)_2O_2^{2-}$. Well-studied base catalyzed silicon sol-gel processes suggest it is reasonable the present Ge-O based gels will exhibit branched structures.[35] Upon aging, condensation reactions involving the remaining Ge-OH moieties are expected form 'GeO_4' tetrahedra as noted in the IR spectra. While the mechanism for the formation of crystalline GeO_2 structures is difficult, and perhaps even impossible to conclusively identify, it is reasonable that a combination of the established solubility (albeit low) of "GeO_2-like" species in basic water and the stabilization afforded by the lattice energy of α-GeO_2 (i.e., 12828 kJ•mol^{-1})[39,40] will lead to the reorganization of the 'GeO_4' tetrahedra and the formation of the thermodynamically favorable crystalline structures presented.

The effect of reaction time and temperature were also investigated. Not surprisingly, based upon isolated yield increasing the temperature pushes the reaction to completion (See Figure S4). These observations may be understood in the context of the equilibrium summarized in Eq. 2 being shifted to the right. These reactions form GeO_2-like sol-gel products that in turn evolve (vide supra) to form crystalline GeO_2 nanocubes. Nanostructures obtained within a short time (0-2 h for 23 °C, 0-15 minutes for 60 °C) of adding TEOG are faceted and clearly based upon a "cube-like" structural motif (See Figure S5 A). Upon solution aging (2- 20 h for 23 °C and 15 min-2 h for 60 °C) in the reaction mixture, nanoparticle shapes evolve to form well-defined cubes (See Figures S5 B, 1G, and H). Again, the limited water solubility of GeO_2 plays a role and is expected to lead to the selective dissolution of high surface energy facets on the randomly shaped structures. Consistent with an Ostwald ripening like process,[37] we also note the appearance of large (edge dimension ca. 5 µm) faceted structures and an apparent shrinkage of the cubes (See Figure S5 C) after extended solution aging (>24 h for 23 °C >6 h at 60 °C).

In conclusion, we have reported a facile method for preparing GeO_2 NPs of tailored shape without the use of surfactants. The morphologies, (i.e., pseudospherical particles, eggs, spindles, and nanocubes) were readily tailored by changing water/ethanol ratios during the hydrolysis of TEOG. Uniform GeO_2 nanocubes with narrow size distribution were obtained by optimizing the concentration of the ammonium hydroxide catalyst.

Acknowledgements

The authors recognize generous continued funding from the Natural Sciences and Engineering Research Council of Canada (NSERC), Canada Foundation for Innovation (CFI), and University of Alberta Department of Chemistry. K. Cui (NINT), G. Popowich and G. Braybrook are thanked for assistance with HRTEM, TEM and SEM, respectively. Dr. M. Iqbal, Dr. Y. Khaniani and the members of the Veinot research team are also thanked for useful discussions.

Notes and references

Department of Chemistry, University of Alberta, 11227 Saskatchewan Drive, Edmonton, Alberta, Canada. Fax: +1-780-492-8231; Tel: +1-780-492-7206, E-mail: jveinot@ualberta.ca

† Electronic Supplementary Information (ESI) available: Details of synthetic procedures and more spectral data and electron microscope images from GeO_2 NPs. See DOI: 10.1039/b000000x/

1 Kahan, *J. App. Phys.*, 1971, **42**, 4444.
2 M. Hoffman and J. G. C. Veinot, *Chem. Mater.*, 2012, **24**, 1283–1291.
3 H. Takeuchi, A. Wung, X. Sun, R. T. Howe, T. King, *J. IEEE Trans. Electron Devices,* 2005, **52**, 2081.
4 H. Hsu, Y. D. He, S. F.Yang, *Cryst. Res. Technol.,* 2011, **46**, 65.
5 Phani, D. Di Claudio, M. Passacantando, S. Santucci, *J. Non-Cryst. Solids* 2007, **353**, 692.
6 Z. Y. Lin and B. K. Garside, *Appl. Opt.* 1982, **21**, 4324.
7 M. Zacharias, P.M. Fauchet, *J. Non-Cryst. Solids,* 1998**, 227**, 1058.
8 Y. Maeda, *Phys. Rev. B*, 1995, **51**, 1658.
9 X. C. Wu, W. H. Song, B. Zhao, Y. P. Sun, J. Du, *J. Chem. Phys. Lett.* 2001, **349**, 210.

10 S. Zyubin, A. M. Mebel, S. H. Lin, *J Phys. Chem. A,* 2007, **111**, 9479.
11 S. Zyubin, A. M. Mebel, S. H. Lin, *J. Chem. Phys.* 2006, **125**, 064701.
12 M. Peng, Y. Li, J. Gao, D. Zhang, Z. Jiang, X. Sun, *J Phys. Chem. C,* 2011, **115**, 11420.
13 Y. Chiu, M. H. Huang, *J. Phys. Chem. C,* 2009, **113**, 6056.
14 S. V. Patwardhan, S. Clarson, *J. Polymer,* 2005, **46**, 4474.
15 P. Kitschke, S. Schulze, M. Hietschold, M. Mehring, *Main Group Met. Chem.*, 2013, **36**, 209.
16 Y. H. Tang, Y. F. Zhang, N. Wang, I. Bello, C. S. Lee, S. T. Lee, *App. Phys. Lett.*, 1999, **74**, 3824.
17 P. Hidalgo, B. Mendez, J. Piqueras, *Nanotechnology*, **2007**, 18, 155203.
18 P. Viswanathamurthi, N. Bhattarai, H.Y. Kim, M.S. Khil, D.R. Lee, E.-K. Suh, *J. Chem. Phys.,* 2004, **121**, 441.
19 K. Saito, A. Ikushima, A. *J. Appl. Phys. Lett.* 1997, **70**, 3504.
20 M. J. Werner, S. R. Fribery, *Phys. Rev. Lett.* 1997, **79**, 4143.
21 V. V. Atuchin, T. A. Gavrilova, S. A. Gromilov, V. G. Kostrovsky, L. D. Pokrovsky, I. B. Troitskaia, R. S. Vemuri, G. Carbajal-Franco, C. V. Ramana, *Cryst. Growth Des.,* 2009, **9**, 1829.
22 Z. Jiang, T. Xie, G. Z. Wang, X. Y. Yuan, C. H. Ye, W. P. Cai, G. W. Meng, G. H. Li, L. D. Zhang, *Mater. Lett.*, 2005, **59**, 416.
23 M. A. Khan, T. P. Hogan, B. Shanker, *J. Raman Spectrosc.,* 2008, **39**, 893.
24 M. Farhan, M. Khan, T. P. Hogan, *J. Alloys Compd.* 2010, **508**, 21.
25 Z. Yang, J. G. C. Veinot, *J. Mater. Chem.*, 2011, **21**, 16505.
26 X. Chen, Q. Cai, J. Zhang, Z. Chen, W. Wang, Z. Wu, *Mater. Lett.,* 2007, **61**, 535–537.
27 H. Wang, Y. Tao, G. Q. Zhang, Y. P. Xia, F. H. Gong, H. P. Wu, and G. L. Tao, *Materials Science Forum*, 2011, **688**, 135–140.
28 H. P. Wu, J. F. Liu, M. Y. Ge, L. Niu, Y. W. Zeng, Y. W. Wang, G. L. Lv, L. N. Wang, G. Q. Zhang, J. Z. Jiang, *Chem. Mater.* 2006, **18**, 1817.
29 T. Kawai, Y. Usui, and K. Kon-no, *Colloids Surf., A,* 1999, **149**, 39.
30 H. Wang, J. F. Liu, H. P. Wu, Y. He, W. Chen, Y. Wang, Y. W. Zeng, Y. W. Wang, C. J. Luo, J. Liu, T. D. Hu, K. Stahl, and J. Z. Jiang, *Journal of Physics: Condensed Matter*, 2006, **18**, 10817–10824.
31 T. M. Davis, M. Snyder, M. Tsapatsis, *Langmuir*, 2007, **23**, 12469.
32 Y. Li, H. S. Lim, S. C. Ng, M. H. Kuok, M. Y. Ge, J. Z. Jiang, *App. Phys. Lett.,* 2007, **91**, 093116.
33 J. D. Rimer, D. D. Roth, D. G. Vlachos, R. F. Lobo, *Langmuir*, 2007, **23**, 2784.
34 Powder Diffraction File (PDF). International Centre for Diffraction Data (ICDD), Newtown Square, PA.
35 U. Schubert, N. Hüsing, *Synthesis of Inorganic Materials*, Wiley, Weinheim, 3rd edn., 2012.
36 G. S. Pokrovski, J. Schott,. *Geochim. Cosmochim. Acta* 1998, **62**, 1631.
37 W. Ostwald, *Lehrbuch der Allgemeinen Chemie,* Leipzig, Germany, 1896.
38 J. Glinnemann, H. E. King, H. Schulz, T. Hahn, S. J. La placa, f. Dacol, *Zeitschrift für Kristallographie*, 1992, **198**, 177.
39 E. Ghobadi, J. A. Capobianco, *Phys. Chem. Chem. Phys.,* 2000, **2**, 5761.
40 CRC handbook of chemistry and physics, Cleveland, Ohio, 2000.